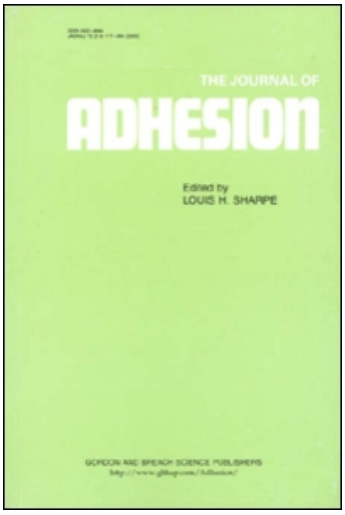

The Journal of Adhesion
Publication details, including instructions for authors and subscription information:
http://www.informaworld.com/smpp/title~content=t713453635

A Progressive Damage Model for the Prediction of Fatigue Crack Growth in Bonded Joints

A. Pirondi[a]; F. Moroni[a]
[a] Industrial Engineering Department, University of Parma, Parma, Italy

Online publication date: 10 June 2010

To cite this Article Pirondi, A. and Moroni, F.(2010) 'A Progressive Damage Model for the Prediction of Fatigue Crack Growth in Bonded Joints', The Journal of Adhesion, 86: 5, 501 — 521
To link to this Article: DOI: 10.1080/00218464.2010.484305
URL: http://dx.doi.org/10.1080/00218464.2010.484305

The Journal of Adhesion, 86:501–521, 2010

ISSN: 0021-8464 print/1545-5823 online
DOI: 10.1080/00218464.2010.484305

Taylor & Francis
Taylor & Francis Group

A Progressive Damage Model for the Prediction of Fatigue Crack Growth in Bonded Joints

A. Pirondi and F. Moroni
Industrial Engineering Department, University of Parma, Parma, Italy

A procedure to predict fatigue crack growth in bonded joints is developed in this work within the framework of cohesive zone modelling and finite element analysis. The idea is to link the fatigue damage rate in the cohesive elements to the macroscopic crack growth rate through a damage homogenisation criterion. In this way, the experimental crack growth rate is related directly to damage evolution in the cohesive zone, that is, no additional parameters have to be tuned beside the quasi-static cohesive zone parameters. The procedure was implemented in the ABAQUS finite element software using the USDFLD subroutine. In order to evaluate the crack growth rate automatically, the strain energy release rate (crack driving force) was calculated and updated automatically within the subroutine. Mode I and Mode II loading cases have been dealt with and the implementation for Mixed Mode I/II is under way.

Keywords: Adhesive bonding; Cohesive zone model; Fatigue; Fracture

1. INTRODUCTION

Fatigue loading is known to be a major source of failures; therefore, an efficient modelling of the fatigue strength, especially for structures designed using a fail-safe or damage-tolerant design method, is fundamental. The fatigue strength is characterized by a number of cycles to failure which is the sum of the time necessary to nucleate the crack and the time to propagate it to rupture. The crack nucleation phase,

Received 22 June 2009; in final form 7 December 2009.
Presented in part at the 3rd International Conference on Advanced Computational Engineering and Experimenting (ACE-X 2009), Rome, Italy, 22–23 June 2009.
Address correspondence to Alessandro Pirondi, Industrial Engineering Department, University of Parma, v. le. Usberti 181/A, 43124 Parma, Italy. E-mail: alessandro.pirondi@unipr.it

for a given average stress, is strongly influenced by the presence and the shape of a fillet or spew at the edge of the joint, as shown in [1–3], while the duration of the propagation phase is related to the length and the shape of the joint [4].

In the case of theoretically defect-free joints, the crack nucleation problem can be studied in terms of local stress in the adhesive layer, or of notch-stress intensity factor (N-SIF) and stress singularity at the corner between adhesive and adherend [4,5]. In the absence of a fillet or spew, or in presence of defects due to lack of polymerisation or adhesion, the nucleation phase is likely to be short, as detected in [1,6]. In this case, the fracture mechanics (FM) approach to fatigue has been extensively tested [7–12]. The fatigue crack growth (FCG) rate da/dN is related to the range of strain energy release rate, ΔG, by an analytical relationship, that can be used to approximate the experimental behaviour. The simplest one is a Paris-like equation,

$$\frac{da}{dN} = C(\Delta G)^m. \tag{1}$$

while a more sophisticated relationship

$$\frac{da}{dN} = D(G_{\max})^{\eta} \frac{1 - \left(\frac{G_{th}}{G_{\max}}\right)^{n_1}}{1 - \left(\frac{G_{\max}}{G_c}\right)^{n_2}} \tag{2}$$

was used in other works such as in [7–9] to account for smooth transitions towards a threshold and an upper bound for the FCG (C, m, D, η, η_1, and η_2 are constant material parameters). In Eq. (2) the FCG driving parameter is the maximum value of G during the loading cycle, G_{max}, instead of ΔG.

The strain energy release rate is a function of crack length, a, that can be evaluated analytically in the case of simple geometries, or by numerical methods such as the finite element (FE) method [7–11,13] in more complex cases. Techniques used to derive G with a FE analysis rely on the calculation of the J-integral or the virtual crack extension (VCE) or the virtual crack closure (VCC) techniques. Once G has been evaluated, a new crack front has to be defined by moving the mesh or by debonding nodes at the crack tip. Crack extension direction and step have to be correctly formulated, and this is not straightforward, especially for 3-D cracks, where the crack driving force and the propagation angle vary across the crack front. Some freeware and commercial FE software (FRANC 2D/3D, ZenCrack, Marc, for example) can do this work automatically in the case of cracks in homogenous bodies, while the case of bonded interfaces is not at the same stage of development.

An efficient way to simulate the presence and the evolution of a defect at a bonded interface is to incorporate a model of the rupture process (*i.e.*, the criterion to trigger propagation) into the finite elements. In particular, the fracture under monotonic loading of bonded joints has been successfully simulated using the cohesive zone (CZ) model (a selection of papers is represented by [14–19]) that is incorporated into the so-called cohesive finite elements. According to this approach, the zone in front of the physical crack tip opens (slides) and then tears progressively apart following a given traction (shear) – separation (sliding) behaviour. The results are generally equivalent to those obtained by other FM techniques listed above, since the CZ parameters are physically related to the fracture toughness, G_c, and the critical crack tip opening displacement, δ_c. Besides, they are often calibrated using the results of fracture experiments. The advantages of using a CZ model are that the evolution of a 3-D crack comes out automatically from the analysis and it is possible to model cases without an initial crack (in this case parameters may not be the same as for cracked bodies as underlined, for example, in [20–22]).

The CZ model was recently used to model fatigue crack growth both in homogeneous bodies [23–25] and at bonded interfaces [26–28] as a convenient alternative to the traditional FM techniques. The work of Yang *et al*. [23]. was based on the BEM (boundary element method). In this case, they defined the evolution law of the stiffness attached to the displacement jump between crack faces in the form of a polynomial expansion, different for loading and unloading cases. The parameters of the evolution law have to be evaluated experimentally with *in-situ* measurements of the traction-crack displacement jump during a cyclic test. Maiti and Geubelle [24] developed a cohesive model that combines damage due to monotonic loading and an evolution law for cohesive stiffness and crack opening displacement as a function of the number of cycles. The two parameters characterizing the fatigue part of the cohesive model can be calibrated by comparison between FE modeling and FCG experimental data. The paper of Ural *et al.* [25]. used a damage degradable cohesive stiffness and a damage evolution law which considered the possibility of damage healing if the surface traction falls below a threshold. In this way, FCG retardation effects due to overload could be modeled. With an adequate calibration of parameters, the model was able to capture both standard FCG data and overload effects.

Concerning interfaces, Roe and Siegmund [26] introduced a cyclic degradation of the monotonic cohesive strength based on a damage variable, D, representing the ratio between the effective (damaged) and nominal (undamaged) cross-section of a representative interface element. The cyclic damage evolution law contained two additional

parameters to be calibrated by FCG experiments. An approach similar to [24] was developed in [27], where the robustness of the model in predicting crack growth rate was demonstrated, with an upper bound for the cohesive element length and number of cycles per increment in order to preserve the accuracy. Differently from other models that require the calibration of cohesive law parameters for cyclic loading, Turon *et al.* [28]. introduced the experimental FCG rate directly into cyclic damage evolution in the cohesive zone through a damage homogenisation criterion. In this way, no parameters have to be tuned in experiments, while the homogenisation criterion becomes a critical issue concerning the performance of the model. Additionally, the value of the applied strain energy release rate must be input to the model, which is not straightforward in the case of complex geometries (in [28] only geometries with a known solution for G were considered). It is worth underlining that in [23,25,26], damage evolution is simulated on cycle-by-cycle basis, while the schemes proposed in [24,27,28] work incrementally on cycles and are, therefore, less expensive from the computational point of view.

This work would like to retain the positive aspect of the work of [28], that is, no need of fatigue parameters calibration but, at the same time, to overcome the problem of the computation of the applied G with the development of an automated procedure based on the global strain energy output issued by the FE analysis. Additionally, a damage definition alike [26] was proposed that allows reproduction the fatigue crack growth experiments more closely than in [28]. The procedure was implemented so far for pure Mode I and pure Mode II, and validated against the corresponding FCG experiments on bonded joints.

2. THEORETICAL FRAMEWORK

The cohesive zone model relates the opening at the crack tip to the stresses at the interface. Considering, for example, only the Mode I, the normal stress-opening relationship is characterized by an ascending branch without development of damage, followed by a descending branch where damage occurs. A simple representation of this characteristic is a triangular shape law, Fig. 1.

Increasing monotonically the opening from 0 to δ_0, the fracture is characterized by a stiffness, K_0. Beyond the opening value corresponding to δ_0, the response of the interface is characterized by a damage value, D, that reduces the stiffness per unit area, K, with respect to the initial one, following the equation

$$K = (1 - D)K_0 \tag{3}$$

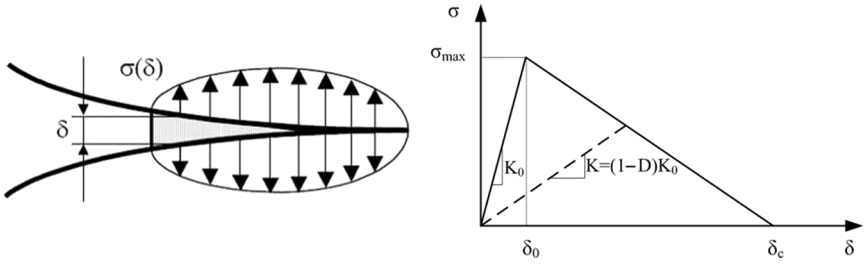

FIGURE 1 Stresses at the crack tip.

until δ_c, where the interface cannot carry load any longer. The energy, Γ, absorbed in this process is equal to the area of triangle

$$\Gamma = \frac{1}{2}\sigma_{\max}\delta_c \tag{4}$$

and it is representative of the fracture energy of the material, G_c.

Considering the damage simply dependent from the opening, the damage variable, D, can be written as

$$D = \frac{\delta_c(\delta - \delta_0)}{\delta(\delta_c - \delta_0)}. \tag{5}$$

Unloading from a damaged condition occurs along the dashed path in Fig. 1. When applying a cohesive zone for monotonic loading to fatigue, two problems arise: i) damage occurs only above the threshold δ_0, which may not be the same for monotonic and fatigue loading; ii) above δ_0 the cycle tends rapidly to shakedown along the dashed unloading path in Fig. 1; therefore, no crack increment is modeled.

The approach proposed in this work to model fatigue damage is of the incremental type, that is, subcritical fatigue damage accumulation rate is related to the increment in the number of cycles. The monotonic behavior is recovered according to the general scheme described previously [Eqs. (3–5)].

Damage is representative of the effect of micro void nucleation and micro-cracks. In general, considering a representative surface element (RSE), as shown in Fig. 2, with a nominal surface equal to A_e and a damaged area due to micro-voids or micro-cracks equal to A_d, D can be written as reported in [29]

$$D = \frac{A_d}{A_e} \tag{6}$$

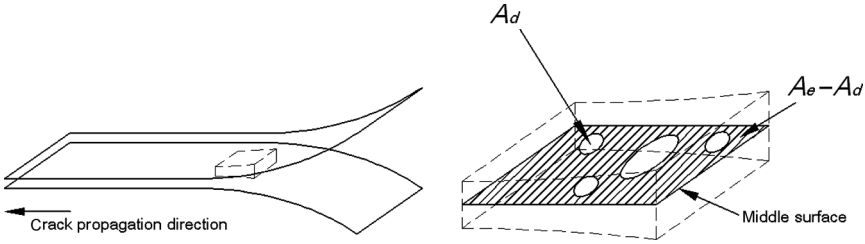

FIGURE 2 Representation of damaged area A_d and initial area A_e for a RSE.

and, therefore

$$\frac{K}{K_0} = 1 - \frac{A_d}{A_e}. \tag{7}$$

The underlying assumption in the use of a RSE instead of a representative volume element (RVE) to characterise damage and its effects is that, since the thickness of the bondline is generally very small (of the order of tenths of millimetres), the distribution of damage is constant through the thickness. In [28], the fatigue crack area extension, dA, is taken as the sum of the damaged area, dA_d, for all of the RSE undergoing damage, that is, the ones within the process zone, A_{CZ}:

$$dA = \sum_{i \in A_{CZ}} dA_d^i. \tag{8}$$

In this work, the middle surface associated with the integration point (IP) of the cohesive element is taken as RSE; therefore, the crack extension is the sum of the damaged area of all of the IPs within A_{CZ}. In 2-D, A_{CZ} reduces to a length, L_{CZ} that may be estimated analytically using a closed form equation [Eq. (9)] coming from Rice [30]

$$L_{CZ} = b \frac{9\pi}{32} \frac{E G_{\max}}{\sigma_{\max}^2}, \tag{9}$$

where b is the width of the crack front, G_{max} is the maximum strain energy release rate in the loading cycle, E is the Young's modulus of the adherends material, and σ_{max} is the maximum cohesive strength. In this work, the process area (A_{CZ}) is taken as the area where the opening is greater than a threshold value (δ_k^{th}, where k is the mode of fracture). Experimentally, the threshold is determined by progressively decreasing ΔG until da/dN falls below a given, low value. The value of ΔG at threshold, ΔG_{th}, is taken as a material parameter.

The cohesive threshold parameter should be determined accordingly, that is, for a fatigue running crack where the cohesive zone has attained a steady-state extension. On the other hand, the value chosen for δ_k^{th} affects, in turn, the extension of the cohesive zone; therefore, a unique solution cannot be found in this way. As a compromise, in this work, δ_k^{th} has been taken equal to the maximum opening (or sliding) within the cohesive zone, when the strain energy release rate applied to the joint is equal to the experimental strain energy release rate threshold (that is $\Delta G = \Delta G_{th}$), before starting the propagation phase.

In order to represent the crack growth due to fatigue, the local damage of the cohesive elements has to be linked to the number of cycles. The fatigue crack growth rate (dA/dN) is represented by Eq. (1) (which was considered in this work) or by more complex expressions like Eq. (2).

The damage growth rate can be written as

$$\frac{dD}{dN} = \frac{dD}{dA_d}\frac{dA_d}{dN}. \tag{10}$$

Deriving Eq. (6), the increment of damage per increment of damaged area for each IP is equal to

$$\frac{dD}{dA_d} = \frac{1}{A_e}. \tag{11}$$

The derivative of Eq. (8) with respect to the number of cycles yields

$$\frac{dA}{dN} = \sum_{i \in A_{CZ}} \frac{dA_d^i}{dN}. \tag{12}$$

The distribution of damage rate across ACZ is neither theoretically nor experimentally easy to evaluate. The points closer to the crack tip can be expected to undergo a higher damage rate than the others located at the end of the process zone, leading, therefore, to a gradual variation of damage along this region. One way could be to infer the trend of damage rate by the comparison of experimental and simulated compliance, but the experimental scatter and the numerical approximation will probably not allow a punctual definition of the damage evolution. On the other hand, a micromechanical analysis is very demanding and the distribution of damage should be sampled at different positions along the crack front. In order to overcome these difficulties, the assumption made in [28] of taking $\frac{dA_d}{dN}$ as the mean value of the damaged area growth rate $\frac{dA_d^i}{dN}$ at the IPs belonging to ACZ allows Eq. (12) to be written as

$$\frac{dA}{dN} = \sum_{i \in A_{CZ}} \frac{dA_d}{dN} = n_{CZ} \frac{dA_d}{dN} = \frac{A_{CZ}}{A_e} \frac{dA_d}{dN}, \tag{13}$$

where n_{cz} is the number of IPs lying on the process area that can be rewritten as the ratio between the process area, A_{CZ}, and the average cross-sectional area associated with cohesive element IPs, A_e. From Eqs. (10), (11), and (13), the fatigue damage growth rate can be computed as:

$$\frac{dD}{dN} = \frac{1}{A_{CZ}} \frac{dA}{dN} = \frac{1}{A_{CZ}} C \Delta G^m \tag{14}$$

3. FINITE ELEMENT IMPLEMENTATION

The framework described previously has been implemented in the FE software ABAQUS (Dassault Systèmes, Providence, RI, USA) using the associated USDFLD subroutine to apply damage to the initial stiffness, K_0.

Assuming that in the fatigue cycle the load varies from a maximum value P_{max} to a minimum value P_{min}, the load ratio is defined as

$$R = \frac{P_{max}}{P_{min}}. \tag{15}$$

The amplitude of the strain energy release rate is computed as

$$\Delta G = (1 - R^2) G_{\max}, \tag{16}$$

where G_{max} is the strain energy release rate extrapolated from the stress and displacement field when the maximum load is applied. The value of ΔG is compared with the fatigue crack growth threshold, ΔG_{th}. If $\Delta G > \Delta G_{th}$, the propagation will take place; otherwise, the analysis is stopped and no more propagation will be shown.

According to the flow diagram in Fig. 3, at the beginning of the increment, n, the damage D_i^n in IPs belonging to the process zone, A_{CZ}, is increased by a given quantity, ΔD_i^n. This quantity is computed following Eq. (17) and it represents the minimum between the required quantity to reach unity and a defined value, ΔD_{max}:

$$\begin{aligned} \Delta D_i^n &= \Delta D_{\max} \quad \text{if } 1 - D_i^n > \Delta D_{\max} \\ \Delta D_i^n &= 1 - D_i^n \quad \text{if } 1 - \mathrm{D}_i^n < \Delta D_{\max}. \end{aligned} \tag{17}$$

The value of ΔD_{max} can be tuned in order to minimize crack growth rate oscillations. For each IP, integrating Eq. (14), an increment in the

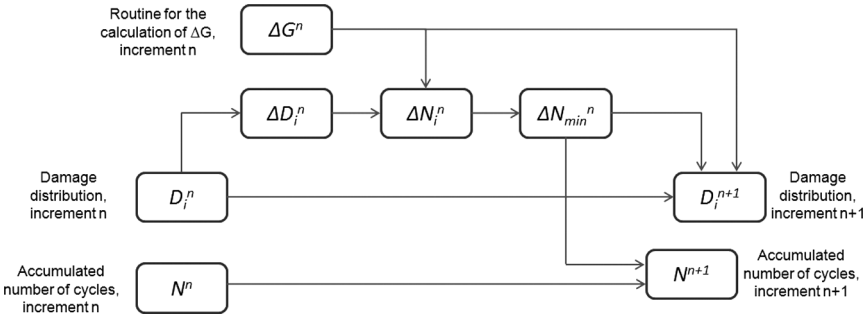

FIGURE 3 Flow diagram of the damage increment.

number of cycles for each one of the IPs, ΔN_i^n is then estimated. After that, the routine searches for the minimum value among the calculated ΔN_i^n. This value, ΔN_{min}^n, is assumed to be the equivalent number of cycles of the increment. Therefore, the number of cycles is updated (N^{n+1}); using Eq. (14), the new damage distribution is computed for all the IPs belonging to the process zone (D_i^{n+1}).

3.1. Strain Energy Release Rate Calculation

In order to know the macroscopic crack growth rate according to Eq. (1), the strain energy release rate has to be computed during the crack propagation. Since the contour integral method is not yet available by default for cohesive elements, a J-integral has been implemented in the routine for a 2-D case. The path of the integral is, in this case, the boundary of the cohesive elements (Fig. 4).

The definition of the J integral [31] is

$$J = \int_{\Gamma} \mathbf{n} \cdot [H] \cdot \mathbf{q} d\Gamma, \tag{18}$$

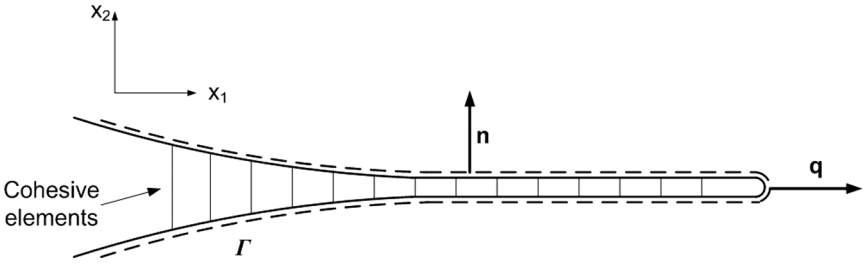

FIGURE 4 Definition of the J integral surrounding the crack tip.

where **n** is a vector normal to the path, **q** is a vector lying on the crack propagation direction, and [H] is defined as

$$[H] = S[I] - [\sigma_{i,j}]\left[\frac{\partial u_{i,j}}{\partial x_{i,j}}\right], \tag{19}$$

where S is the strain energy density, $[\sigma_{i,j}]$ the stress matrix, and u_i the displacements of the points lying on the path. If the crack lays on the plane orthogonal to x_2, and the geometrical non linearity can be neglected, the J integral can be written as

$$J = \int_{\Gamma}\left(-\sigma_{1,2}\frac{\partial u_1}{\partial x_1} - \sigma_{2,2}\frac{\partial u_2}{\partial x_1}\right)d\Gamma. \tag{20}$$

The methodology described above is more difficult to implement in a 3-D case. In this perspective, G has also been computed according to the original Griffith's definition, or energy derivative technique (EDT):

$$G = -\frac{d(U-W)}{dA}. \tag{21}$$

where U is the internal strain energy, while W is the work of the external forces.

This methodology is rather simple and it can be easily applied also to 3-D geometries, but is rather sensitive to the estimation of dA. In particular, if the crack growth between two subsequent increments is not constant, oscillations in the value of G become sensible. Both methods were initially considered, and, for high mesh refinements, they give very similar results. In order to keep the time of the analysis as low as possible, the J-integral methodology was chosen in this phase because it yields stable results also, with a less refined mesh.

4. RESULTS

4.1. Strain Energy Release Rate Calculation

The strain energy release rate calculation procedure has been validated by comparing the results with respect to the analytical solution of G as a function of the crack length for Mode I double cantilever beam (DCB, Fig. 5), Mode II end notched flexure (ENF, Fig. 6), and end loaded split (ELS, Fig. 7) geometries. For all specimens, the adherends were supposed to be of aluminium alloy with an elastic modulus and Poisson's ratio, respectively, equal to $E = 70000\,\text{MPa}$, $\nu = 0.35$. The results refer to a mesh dimension of 1 mm for the adherends and 0.2 mm for the cohesive elements.

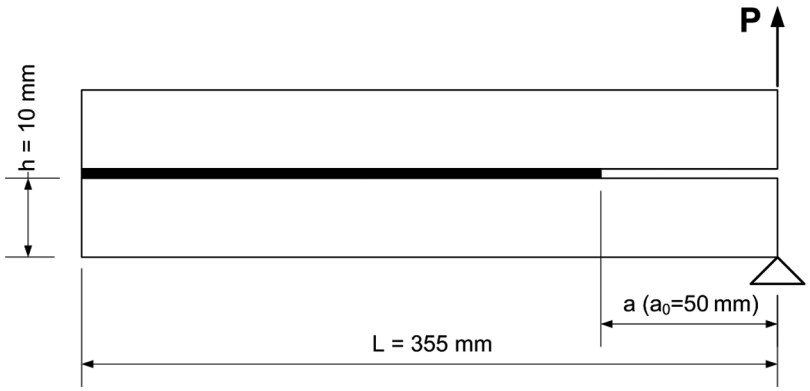

FIGURE 5 DCB geometry.

The adherends were modeled as four-noded plane stress isoparametric, fully integrated elements.

Considering the DCB geometry (Fig. 5), the analytical solution for G taken as reference is

$$G = \frac{(Pa)^2}{bEI}\left(1 + \frac{1}{a\lambda_\sigma}\right)^2, \tag{22}$$

where I is the second moment of area of the beam section ($I = \frac{bh^3}{12}$, b is the width, and h is the thickness of each beam) and λ_σ is a constant parameter depending on the geometry and material properties [32].

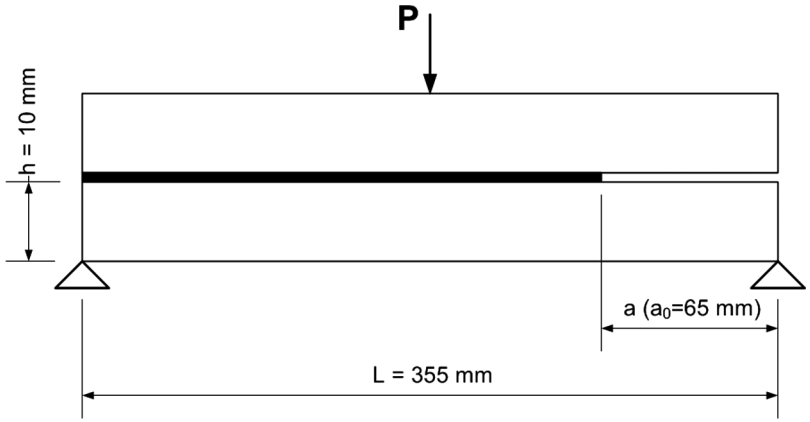

FIGURE 6 ENF geometry.

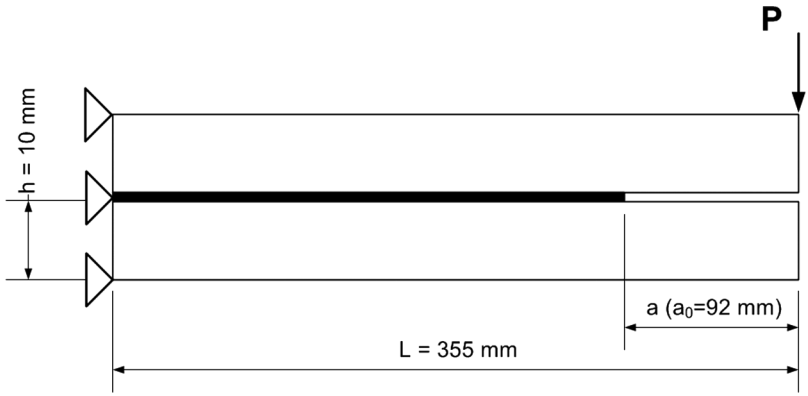

FIGURE 7 ELS geometry.

In the case of the ENF geometry (Fig. 6), the reference is Eq. (23) derived from Wang and Williams [33]:

$$G = \frac{9(a + 0.42\Delta_I)^2 P^2}{16 b^2 E h^3} \tag{23}$$

where Δ_I is a crack length correction to account for the shear deformation, and is equal to

$$\Delta_I = h\sqrt{\frac{2(1+\nu)}{11}\left[3 - 2\left(\frac{\Gamma}{\Gamma+1}\right)^2\right]} \tag{24}$$

with

$$\Gamma = 1.18 \cdot 2(1+\nu). \tag{25}$$

This formulation [Eq. (23)] is valid only for a crack length lower than $L/2$. Finally, the strain energy release rate for the ELS geometry (Fig. 7), derived from Wang and Williams [33], is equal to:

$$G = \frac{9(a + \Delta_{II})^2 P^2}{4 b^2 E h^3}. \tag{26}$$

where $\Delta_{II} = 2\Delta_I$. Figures 8–10 show the comparison between the analytical solution and the strain energy release rate computed using the FCG subroutine developed in this work. In all the three cases, a very good agreement is obtained. For the ENF and ELS joints, some oscillation can be noticed at the beginning of the propagation phase. These are linked to the mesh dimension: the smaller the mesh dimension of adherend and adhesive, the smaller are the oscillations.

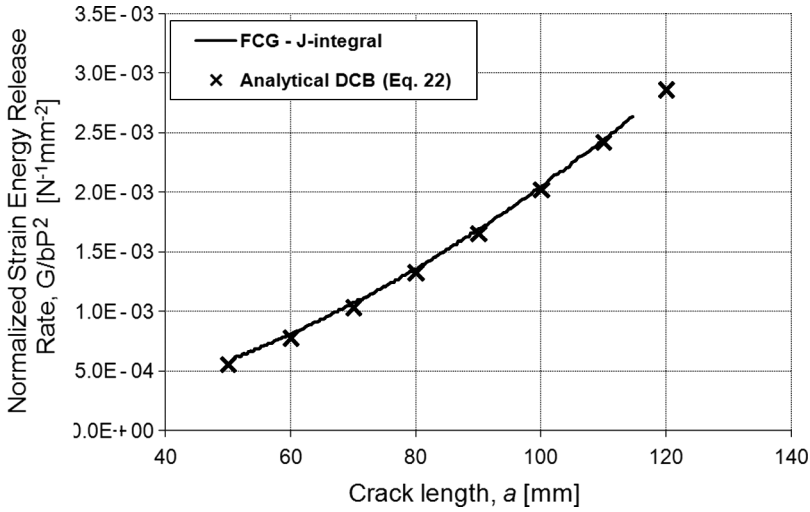

FIGURE 8 Comparison between the normalized strain energy release rate automatically computed by the FCG subroutine and the analytical equation for the DCB joint.

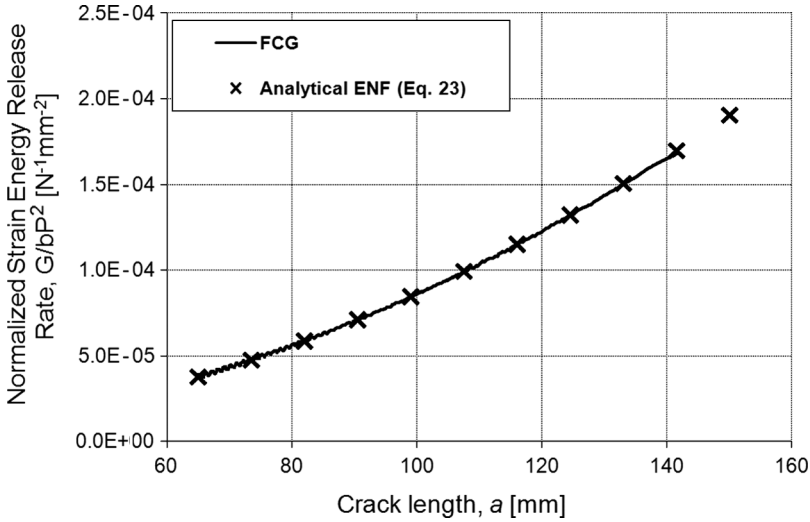

FIGURE 9 Comparison between the normalized strain energy release rate automatically computed by the FCG subroutine and the analytical equation for the ENF joint.

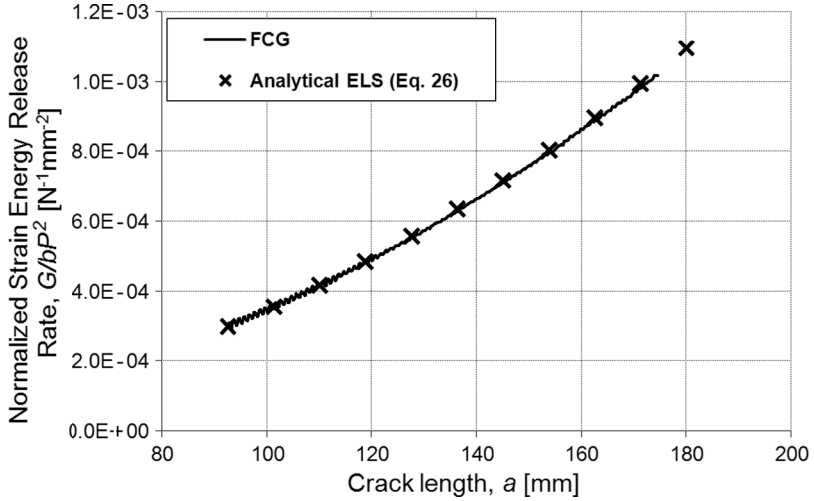

FIGURE 10 Comparison between the normalized strain energy release rate automatically computed by the FCG subroutine and the analytical equation for the ELS joint.

It is also interesting to compare the results obtained using Eqs. (20) and (21). For the same mesh size (DCB joint with a mesh size of 0.2 mm for the cohesive elements, and 1 mm for the adherends), Eq. (21) yields the same trend as Eq. (20) but with evident oscillations, as shown in Fig. 11. A little qualitative improvement can be obtained refining the mesh of adherends and cohesive zone, but in this case a greater computational effort is necessary. Fig. 12 shows, for example, the same analysis carried out for Fig. 11, but with a mesh size of 0.1 mm for the cohesive zone.

4.2. FCG Rate Simulation

The Mode I and Mode II parameters of the cohesive zone and FCG rate were taken from the work of [28], Table 1. The result is the simulated FCG rate, compared with the one calculated analytically with the parameters in Table 2.

The comparison is shown in Figures 13–15 for the three joint geometries (0.2 mm mesh dimension was used for the cohesive zone, 1 mm for the substrates, and a value of ΔD_{max} equal to 0.2). Concerning the Mode I propagation (DCB joint), there is a good prediction of the crack growth rate, but small differences can be noticed regarding the slope of the curve: the FCG rate model gives a curve with a slope

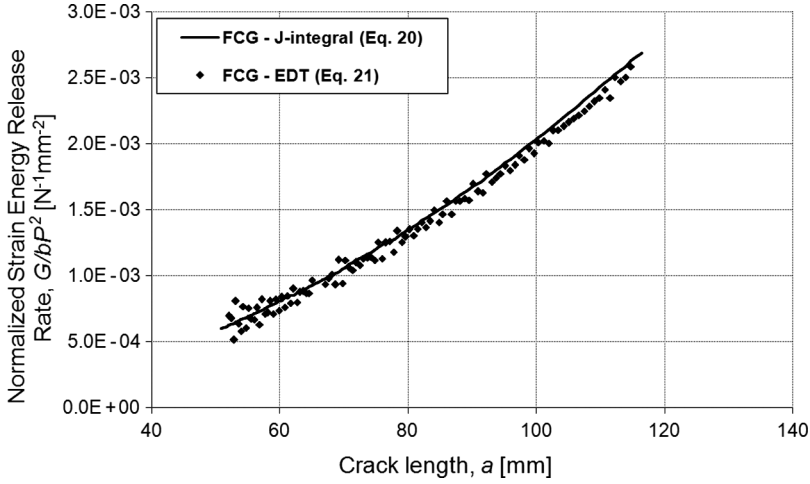

FIGURE 11 Comparison between the normalized strain energy release rate computed by using the J-integral [Eq. (20)] and the EDT [Eq. (21)], for a DCB joint having a mesh size of 0.2 mm for the cohesive zone and 1 mm for the adherends.

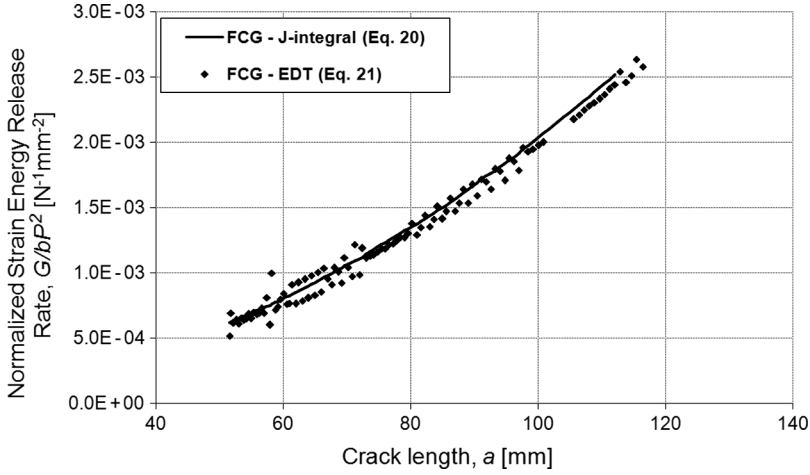

FIGURE 12 Comparison between the normalized strain energy release rate computed by using the J-integral, [Eq. (20)] and the EDT [Eq. (21)], for a DCB joint having a mesh size of 0.1 mm for the cohesive zone and 1 mm for the adherends.

TABLE 1 Cohesive Zone Parameters, Similar to [28]

Parameters		Mode I	Mode II
Fracture energy	Γ [N/mm]	0.260	1.00
Maximum stress	σ [MPa]	30	30
Critical opening	δ_c [mm]	0.0173	0.666
Onset damage opening	δ_0 [mm]	0.003	0.003

TABLE 2 FCG Rate Parameters, Similar to [28]

	Mode I	Mode II
C	0.0616	4.23
M	5.4	4.5
G^{th} [N/mm]	0.06	0.100

slightly lower than that obtained with the reference parameters. A qualitatively similar, even more pronounced behavior has been evidenced also in [28]. The difference with respect to that work is related to the different definition of damage [Eq. (6)] used here, where D affects K_0 instead of Γ_0 as in [28].

Concerning Mode II, both ENF and ELS geometries seem to give a very good prediction of the crack growth rate, even though a small

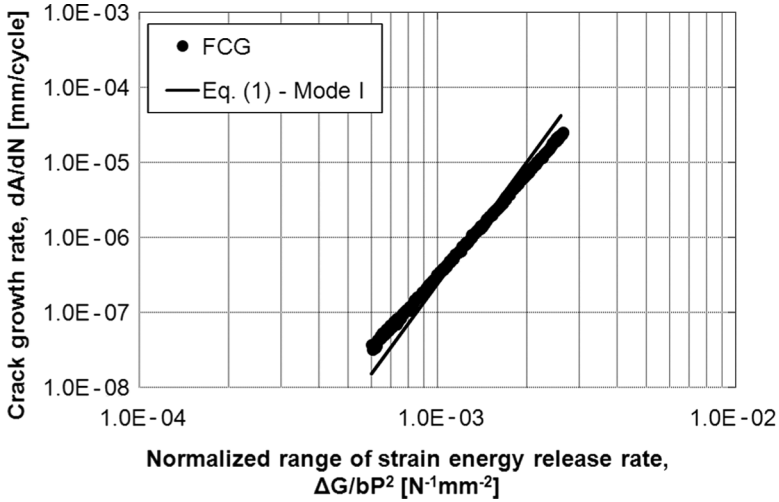

FIGURE 13 Comparison between the crack growth rate trend computed by the FCG subroutine and the reference trend for the DCB joint.

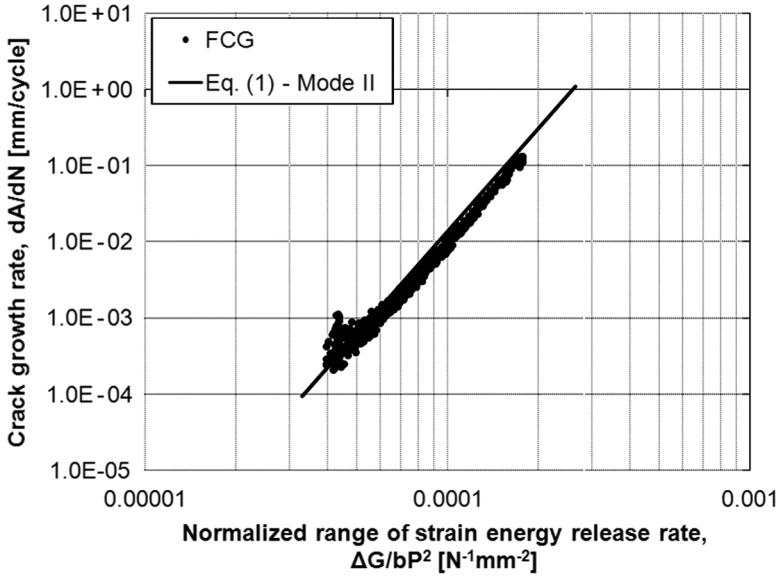

FIGURE 14 Comparison between the crack growth rate trend computed by the FCG subroutine and the reference trend for the ENF joint.

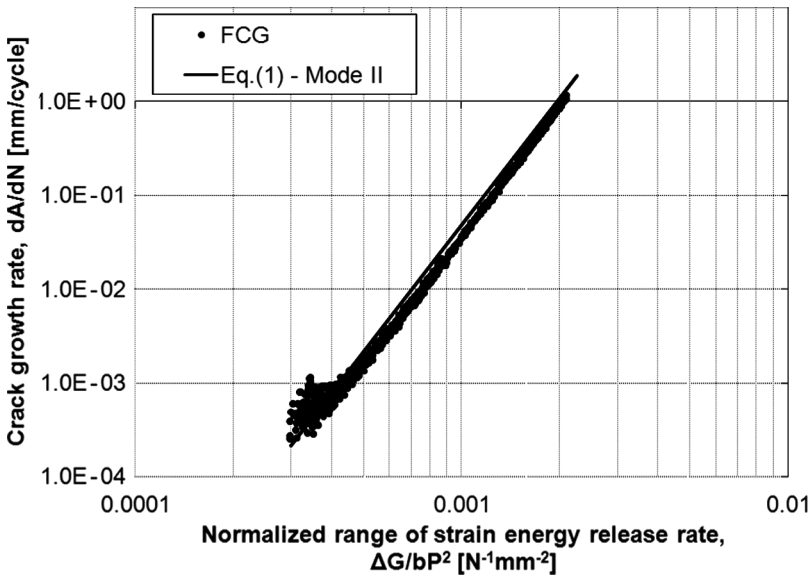

FIGURE 15 Comparison between the crack growth rate trend computed by the FCG subroutine and the reference trend for the ELS joint.

reduction of the slope with respect to the reference curve can also be found in this case. Moreover, in the initial phase, the development of the cohesive zone at the crack tip yields small perturbancies in the crack length calculation that result in some oscillation of the crack growth rate.

Finally, an insight into the influence of two fundamental parameters of the analysis, *i.e.*, cohesive element size and damage increment ΔD_{max}, has been provided.

Concerning the cohesive mesh size, as it slightly affects the J-integral computation, in the same manner the dA/dN *vs.* ΔG plot is slightly affected by the mesh size as shown in Fig. 16. The cohesive zone, in all the cases examined, encompassed at least four to five elements. Therefore, a "rule-of-thumb" of a minimum number of cohesive elements within the process zone A_{CZ}, which is well established in the monotonic loading case, seems to hold also for the fatigue crack growth case.

Figure 17 shows the influence of ΔD_{max} on the crack growth rate. While the slope is preserved, the fatigue crack growth rate decreases for an increase of ΔD_{max}, and this is more evident at low values of ΔG. Moreover, it can be observed that the extension of the cohesive zone decreases when ΔD_{max} increases, yielding a poor representation

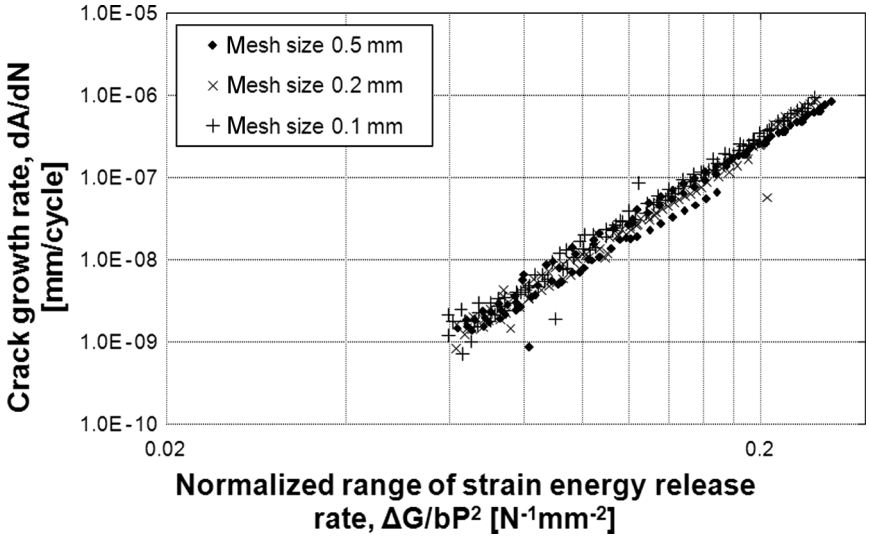

FIGURE 16 Predicted crack growth rate for different cohesive element sizes (DCB joint).

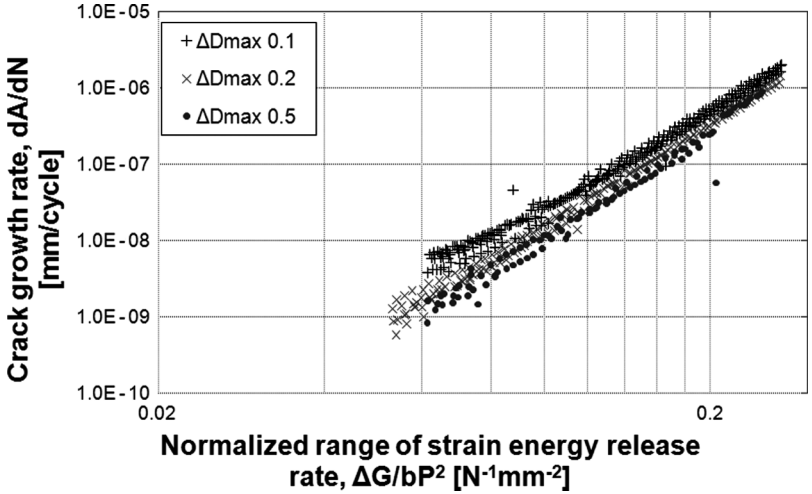

FIGURE 17 Predicted crack growth rate for different values of ΔD_{max} (DCB joint).

of the cohesive zone stresses at the crack tip that, in turn, may affect the fatigue crack growth prediction. Anyway, it is worth remarking that, in the present case, going from $\Delta D_{max} = 0.5$ to $\Delta D_{max} = 0.1$ means to increase the analysis time by a factor of five. The best performance in terms of approximation of the experiments is obtained in this case using $\Delta D_{max} = 0.2$.

5. CONCLUSIONS

In this work, a routine interacting with a finite element software is defined in order to represent the fatigue crack growth in a bonded joint using cohesive elements. The traditional cohesive zone model has been modified in order to model both the monotonic loading damage and the fatigue crack growth rate. An additional feature is the automated evaluation of the strain energy release rate using the contour integral method. The J-integral computation is validated by comparison with analytical solutions for simple joint geometries representing pure Mode I and pure Mode II and, for the same geometries, the fatigue crack growth predictions are compared with literature data. In both cases, good agreement was found, leaving room for the extension to mixed-mode and 3-D loading conditions.

REFERENCES

[1] Dessureault, M. and Spelt, J. K., *Int. J. Adhes. Adhes.* **17**, 183–195 (1997).
[2] Ferreira, J. A. M., Reis, P. N., Costa, J. D. M., and Richardson, M. O. W., *Compos. Sci. Technol.* **62**, 1373–1379 (2002).
[3] Hadavinia, H., Kinloch, A. J., Little, M. S. G., and Taylor, A. C., *Int. J. Adhes. Adhes.* **23**, 449–461 (2003).
[4] Ishii, K., Imanaka, M., Nakayama, H., and Kodama, H., *Compos. Sci. Technol.* **59**, 1675–1683 (1999).
[5] Quaresimin, M. and Ricotta, M., *Int. J. Fatigue* **28**, 1166–1176 (2006).
[6] Krenk, S., Jönsson, J., and Hansen, L. P., *Eng. Fract. Mech.* **53**, 859–872 (1996).
[7] Curley, A. J., Hadavinia, A., Kinloch, A. J., and Taylor, A. C., *Int. J. Fracture* **103**, 41–69 (2000).
[8] Abdel Wahab, M. M., Ashcroft, I. A., Crocombe, A. D., and Smith, P. A., *Int. J. Fatigue* **24**, 705–709 (2002).
[9] Hadavinia, H., Kinloch, A. J., Little, M. S. G., and Taylor, A. C., *Int. J. Adhes. Adhes.* **23**, 463–471 (2003).
[10] Melander, A., Linder, J., Stensiö, H., Larsson, M., Gustavsson, A., and Björkman G., *Fatigue Fract. Eng. M.* **22**, 421–426 (1999).
[11] Abdel Wahab, M. M., Ashcroft, I. A., Crocombe, A. D., and Smith, P. A., *Composites: Part A.* **35**, 213–222 (2004).
[12] Shang, J-K., Fatigue '96 Proceedings of the Sixth International Fatigue Congress, 6–10 May 1996, Berlin, Germany, G. Lutjering and H. Nowack (Ed.) (Pergamon, Tarrytown, NY, 1996).
[13] Pirondi, A. and Moroni, F., *Int. J. Adhes. Adhes.* 29, 796–805 (2009).
[14] Tvergaard, V. and Hutchinson, J. W., *J. Mech. Phys. Solids* **44**, 789–800 (1996).
[15] Yang, Q. D., Thouless, M. D., and Ward, S. M., *J. Mech. Phys. Solids* **47**, 1337–1353 (1999).
[16] Mohammed, I. and Liechti, K. M., *J. Mech. Phys. Solids* **48**, 735–764 (2000).
[17] Ferracin, T., Landis, C. M., Delannay, F., and Pardoen, T., *Int. J. Solids. Struct.* **20**, 2889–2904 (2003).
[18] Li, S., Thouless, M. D., Waas, A. M., Schroeder, J. A., and Zavattieri, P. D., *Eng. Fract. Mech.* **73**, 64–78 (2006).
[19] Martiny, Ph., Lani, F., Kinloch, A. J., and Pardoen, T., *Int. J. Adhes. Adhes.* **28**, 222–236 (2008).
[20] Corigliano, A. and Allix, O., *Comput. Method. Appl. M.* **24**, 185–203 (2000).
[21] Pirondi, A., Influence of cohesive law shape and adhesive modelling on the failure prediction of T-peel joints in *Fracture of Nano and Engineering Materials and Structures* – Proc. ECF 16 Conference, E. E. Gdoutos (Ed.) (Springer, 2006).
[22] Scheider, I., Hachez, F., and Brocks, W., Effect of cohesive law and trixiality dependence of cohesive parameters in ductile learning in *Fracture of Nano and Engineering Materials and Structures* – Proc. of ECF 16 Conference, E. E. Gdoutos (Ed.), (Springer, Heidelberg, 2006).
[23] Yang, B., Mall, S., and Ravi-Chandar, K., *Int. J. Solids. Struct.* **44**, (38), 3927–3944 (2001).
[24] Maiti, S. and Geubelle, P. H., *Eng. Fract. Mech.* **72**, 691–708 (2005).
[25] Ural, A., Krishnan, V. R., and Papoulia, K. D., *Int. J. Solids. Struct.* **46**, 2453–2462 (2009).
[26] Roe, K. L. and Siegmund, T., *Eng. Fract. Mech.* **70**, 209–232 (2003).
[27] Muñoz, J. J., Galvanetto, U., and Robinson, P., *Int. J. Fatigue* **28**, 1136–1146 (2006).

[28] Turon, A., Costa, J., Camanho, P. P., and Dàvila, C. G., *Composites* **38**, 2270–2282 (2007).
[29] Lemaitre, J., *J. Eng. Mater. Tech.* **107**, 83–89 (1985).
[30] Rice, J. R., Mathematical analysis in the mechanics of fracture, in *Fracture*, H. Liebowitz (Ed.) (Academic Press, New York, 1968), Vol. 2, pp. 191–311.
[31] Rice, J. R., *J. Appl. Mech.* **35**, 379–386 (1968).
[32] Krenk, S., *Eng. Fract. Mech.* **43**, 549 (1992).
[33] Wang, W. and Williams, J. G., *Compos. Sci. Technol.* **43**, 251–256 (1992).